Earth and Planetary Science Letters 539 (2020) 116192

Contents lists available at ScienceDirect

Earth and Planetary Science Letters

www.elsevier.com/locate/epsl

Potassium isotope fractionation during chemical weathering of basalts

Heng Chen [a,b,*], Xiao-Ming Liu [c], Kun Wang (王昆) [a]

[a] Department of Earth and Planetary Sciences, Washington University in St Louis, St. Louis, MO 63130, USA
[b] Lamont-Doherty Earth Observatory, Columbia University, Palisades, NY 10964, USA
[c] Department of Geological Sciences, University of North Carolina at Chapel Hill, Chapel Hill, NC 27599, USA

ARTICLE INFO

Article history:
Received 26 February 2019
Received in revised form 24 February 2020
Accepted 28 February 2020
Available online 30 March 2020
Editor: L. Derry

Keywords:
potassium isotopes
chemical weathering
basalt
clay minerals
global potassium cycle

ABSTRACT

Non-traditional stable isotopes (*e.g.*, Li, Mg, and Si) are increasingly used as tracers for studying Earth's surface processes. The isotopes of potassium (K), a highly soluble and mobile element during weathering, could be a promising new tracer for continental weathering; however, the K isotopic variations in weathering profile has not been directly studied due to previous analytical difficulties. Recent high-precision measurements revealed that K isotopes in global river waters are fractionated from the Bulk Silicate Earth (BSE) value, indicating they are influenced by chemical weathering of the crust. Isotopic fractionation during chemical weathering is one of several processes that could ultimately lead to ~0.6‰ difference of δ^{41}K between the BSE and modern seawater. In order to determine the direction and controlling factors of K isotopic fractionation during basalt weathering, especially under intense weathering conditions, we measured K isotopic compositions in two sets of bauxite developed on the Columbia River Basalts, together with fresh parental basalt and aeolian deposit samples using a recently developed high-precision method. Results show that K isotopic variations among fresh basalts and aeolian dust are limited, close to the BSE value. Extreme K depletion (>99%) and K isotopic fractionation (δ^{41}K up to 0.5 ‰) are observed in bauxite drill cores due to intense chemical weathering. The top of the weathering profiles shows less depletion in K abundances and the δ^{41}K values are closer to those of the fresh basalts and aeolian dusts, likely due to addition of aeolian dust at the tops of both profiles. The weathered products are generally depleted in heavy K isotopes, which is consistent with heavier K isotopic compositions observed in river water and seawater. The δ^{41}K in bauxites displays a positive correlation with K_2O contents as well as δ^{7}Li, indicating the behaviors of K and Li isotopes are comparable during chemical weathering. This study shows that K concentrations and its isotopic compositions are sensitive tracers of chemical weathering and could be good weathering proxies over Earth's history.

1. Introduction

Chemical weathering modifies the morphology of the Earth's surface (Meybeck, 1987), regulates the global climate, and provides nutrients necessary for life (Ludwig et al., 1996). Chemical weathering also has a profound influence on the average composition of the continental crust, as it removes mass from the continental crust into the oceans and modifies chemical compositions of the crust and ocean (Suchet et al., 2003; Liu and Rudnick, 2011). Weathering profiles preserved important information regarding Earth's climate and atmospheric compositions (Singer, 1980). Therefore, studies of rock and mineral weathering are significant for pedogenesis and vital in many fields of geology and geochemistry (Nesbitt and Young, 1989).

Overall, the geochemical cycles of cations (*e.g.*, Na, K, and Ca) are predominantly impacted by the processes of chemical weathering, sedimentation, and hydrothermal circulation in the oceans. Historically, the fluxes within the global geochemical cycles were quantified by measurements of elemental concentrations in riverine fluxes and hydrothermal systems as well as the chemical composition of marine sediments (Garrels and MacKenzie, 1971; Berner and Berner, 2012). Uncertainties in these fluxes are usually large due to lack of quantification of certain processes, analytical challenges, and poor global coverage (Berner and Berner, 2012; Fantle and Tipper, 2014). With the development of analytical technique, many non-traditional stable isotope systems have emerged as proxies (*e.g.*, Li, Mg, and Si) for studying the global elemental cycles (Frings et al., 2016; Liu and Rudnick, 2011; Tipper et al., 2006). These stable isotopes provide key constraints on elemental

* Corresponding author.
E-mail addresses: chenheng@levee.wustl.edu, hengchen@ldeo.columbia.edu (H. Chen).

https://doi.org/10.1016/j.epsl.2020.116192
0012-821X/

cycling that cannot be determined solely from elemental concentrations (Fantle and Tipper, 2014).

Potassium is a mobile alkali metal element that moves readily between and within geochemical reservoirs. Despite its relatively high abundance (~400 ppm) and long residence time (~10 Myr) in the oceans, understanding of the global K cycle is limited (Berner and Berner, 2012). Potassium has two stable isotopes (^{39}K and ^{41}K), and its isotopic composition is often reported as δ^{41}K, where $\delta^{41}K_{sample} = [(^{41}K/^{39}K)_{sample}/(^{41}K/^{39}K)_{standard} - 1] \times 1000$. Recent analytical breakthroughs have made precise measurement of ^{41}K/^{39}K possible on multi-collector inductively coupled plasma mass spectrometers (MC-ICP-MS), and the high precision data reveal that seawater and bulk silicate Earth (BSE) have significantly distinct K isotopic composition, as seawater has a δ^{41}K ~0.6‰ higher than the BSE (Chen et al., 2019; Hu et al., 2018; Li et al., 2016; Morgan et al., 2018; Wang and Jacobsen, 2016). This raises a fundamental question: what processes lead to the elevated δ^{41}K value in seawater? Rivers are a major input of the K into the oceans, and K in river water is primarily derived from the weathering of silicate rocks (Berner and Berner, 2012). Chemical weathering is thus a possible fractionation process that could account for the large K isotopic difference between the ocean and crust. Understanding K isotopic behavior during continental weathering is critical in determining the riverine input to the oceans, which may assist in the development of K isotopes in seawater as a proxy of continental weathering through time.

As continental crust is ultimately derived from mantle-derived melts, and primary lavas at convergent margins, where much of the continental crust is generated, are basaltic (Rudnick, 1995). Examining the direction and magnitude of K isotopic fractionation during chemical weathering of basalts is essential in understanding K behaviors during continental weathering. In this study, we measured K isotope ratios in two well-characterized weathering profiles (bauxites) developed on Columbia River Basalts (CRBs), USA. Here we report high-precision K isotopic data of weathering profiles for the first time.

2. Geology and samples

The Columbia River Basalts (CRBs) which erupted in the Miocene (between 17 Ma and 6 Ma) in the US Pacific Northwest, exposed in the U.S. states of Washington, Oregon Idaho, Nevada, and California (**Fig. 1**; Tolan, 1989; Hooper, 1997). Distribution of individual flows in the CRBs has been recognized based on field relationships, geochemistry, and paleomagnetic properties (*e.g.*, Reidel, 1989; Hooper, 1997). Eruptions were most vigorous ~17-14 million years ago, when over 99 percent of the basalt was released. Less extensive eruptions continued until 6 million years ago.

The Cascade Mountain Range dominates the landscape of the Pacific Northwest. The CRBs crop out both east and west of the Cascade Mountain Range. The Cascades developed progressively since the Late Eocene, with topography increasing more or less steadily since the Late Oligocene (Kohn et al., 2002); This topographic increase created two different climate zones that affected the CRBs via the rain shadow effect: the wet-western and dry-eastern regions. Regions west of Cascades have high mean annual precipitation (MAP; 1500–2000 mm), whereas annual precipitation east of Cascades is less than 300 mm (Kohn et al., 2002; Takeuchi et al., 2010).

The two weathering profiles studied here are the same as those investigated in a companion Li and Mg isotope study (Liu et al., 2013, 2014). Paleo-environmental evidence suggests that in the middle to late Miocene, around the time that the CRB eruption, climate in the inland Pacific Northwest was warmer and wetter than today (Takeuchi et al., 2010). The bauxites are products of

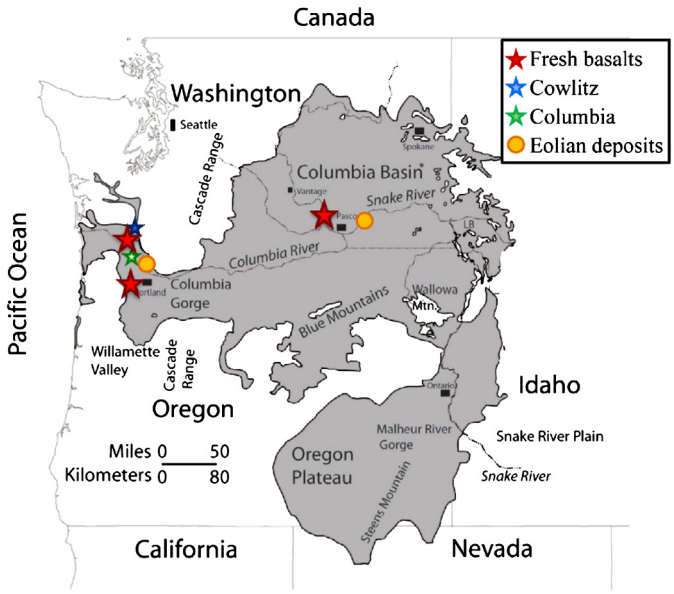

Fig. 1. Map showing the distribution of the Columbia River Basalts (gray) and the locations of samples investigated here. The base map is courtesy of Steve Riedel (Liu et al., 2013).

basalts subjected to extreme weathering conditions. The bauxite units were developed on two different CRB flows and sampled via drill cores: the Sentinel Bluffs Member of the Grande Ronde Basalt in Columbia County, Washington (hereafter referred to as the "Columbia drill core"), and the Pomona Member of the Saddle Mountains Basalt in Cowlitz County, Oregon (hereafter referred to as the "Cowlitz drill core").

Samples measured in this study include (1) two ~10 m drill cores (Cowlitz and Columbia) through bauxites developed on different CRBs basalt flows. All bauxites in this study fall into the extremely weathered category, where Chemical Index of Alteration (CIA) values are extremely high (CIA>98, see **S1**); (2) fresh parental basalts (Sentinel Bluffs basalts and Pomona basalts) upon which the bauxites developed respectively (3) two samples of recent aeolian deposits (Portland Hills Silt and Palouse Formation).

3. Analytical methods

Mineral identification and proportion analysis were previously performed using X-ray Diffraction (XRD) by Liu et al. (2013). The K_2O contents, along with other major and trace elements were analyzed in the same study by X-ray Fluorescence analysis (XRF) and details can be found in Liu et al. (2013).

To measure the K isotopic compositions of bulk samples, ~20-300 mg (depending on K concentration) of powder was digested through a standard two-step protocol (concentrated HF+HNO_3 and 6 N HCl). The fully digested bulk samples were dried down, and a chromatography previously described in Chen et al. (2019) was used to separate K from other elements. Samples dissolved in 1 mL 0.7 N HNO_3 were first loaded on 17 mL columns filled with Bio-Rad AG50W-X8 cation 100-200 mesh exchange resin. Matrix elements were eluted by adding 87 mL 0.7 N HNO_3 and K was recovered into acid-cleaned Teflon beakers by adding 107 mL 0.7 N HNO_3. The recovered K was dried down and re-dissolved with 1 mL 0.5 N HNO_3, and then the process was repeated twice on 2.4 mL columns filled with the same resin to further purify K. The recovered K was dried down and re-dissolved with 5 ml 2% HNO_3 before measurement. The K recovery rate of each column monitored by pre- and post- K-cut is better than 99%. Four total-procedure blanks monitored during the period of this study have an average K of 55 ± 20 ng (2SD; n = 4). Considering total K in

Table 1
Potassium isotopic compositions (δ^{41}K) of selected USGS standards and procedural replicates to test precision and accuracy.

Sample	Lithology	K_2O (wt.%)	δ^{41}K	2s.e.	n[a]
9/3-19	bauxite	0.008	-0.72	0.03	12
9/3-19[#]			-0.73	0.04	10
SB-1	basalt	1.05	-0.63	0.03	11
SB-1[#]			-0.63	0.04	10
2340	basalt	1.23	-0.31	0.02	11
2340[#]			-0.31	0.03	10
2380	basalt	1.19	-0.47	0.04	11
2380[#]			-0.50	0.03	10
2450	basalt	0.98	-0.66	0.03	11
2450[#]			-0.65	0.04	10
BHVO-2	basalt	0.52	-0.47	0.03	79
BHVO-2*			-0.46	0.04	13
BCR-2	basalt	1.79	-0.46	0.03	11
BCR-2*			-0.49	0.05	8

[#] indicate procedural replicates
* Data are from Chen et al. (2019)
[a] n = number of repeat measurements by MC-ICP-MS

each sample is at least 5000 ng, the blank is less than 2% of total K in sample, and therefore not change the isotopes of samples.

After column chemistry, an aliquot of the purified K solution for each sample was diluted for the concentration measurement using a Thermo Scientific iCAP Q ICP-MS. A solution containing 300 ppb of K in 2% HNO_3 was then prepared for isotopic analysis and matched with 300 ppb standard solutions. The difference of concentration between any sample and the standard was consistently less than 1.5%. The K isotopic compositions of all samples were measured using a "dry plasma" setting on a Neptune™ Plus MC-ICP-MS at Washington University in St. Louis. Radio frequency (RF) forward power is set as 1200 W, compared with 600 W or even lower for a "cold plasma" setting (Chen et al., 2019). An Apex Ω high sensitivity desolvating nebulizer made by Elemental Scientific™ was used for sample introduction, and it simultaneously maximizes ICP-MS sensitivity and suppresses the formation of argon hydride (ArH^+). Compared with previous "cold plasma" setting, the "dry plasma" setting used in this study increases the K isotope signals at least 5 times and lowers the ArH^+ to an order of magnitude, therefore, making measurements of low-K samples possible. The Faraday cups in the MC-ICP-MS were positioned to collect the masses of ^{39}K and ^{41}K. The interference of $^{40}ArH^+$ on $^{41}K^+$ can be avoided by measuring Ar-interference-free "shoulder" in high mass resolution mode. A possible $^{40}CaH^+$ isobaric interference was monitored by measuring the intensity of the $^{44}Ca^+$ peak.

The K isotopic composition is reported as δ^{41}K, where $\delta^{41}K_{sample} = [(^{41}K/^{39}K)_{sample}/(^{41}K/^{39}K)_{NIST\_3141a} - 1] \times 1000$, and NIST_3141a is a widely used K isotope standard (Teng et al., 2017). The sample-standard sequence was repeated N times ($N \geq 10$) to reduce instrumental related random error and achieve better reproducibility. The internal (within-run) reproducibility is typical ~0.05‰ or better. The long-term (~12 months) reproducibility of this method has been evaluated as better than 0.10‰ (2σ). In order to further test the reproducibility of our sample digestion and analysis techniques, total procedural replicates of 5 samples were measured three months after our first measurements. The δ^{41}K variations between replicates of the same sample are within ≤0.03‰, demonstrating excellent reproducibility. The USGS geostandards measured in this study require less amount of sample, however achieved comparable isotopic results compared with previous studies by using "cold plasma" setting (see **Table 1** and summarization in Chen et al., 2019).

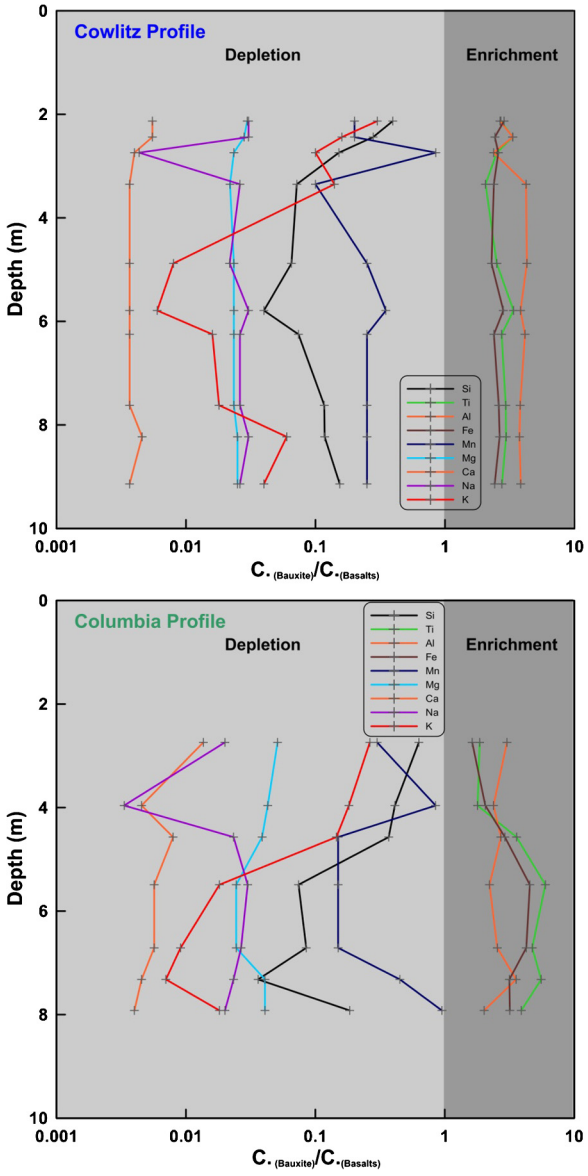

Fig. 2. Concentrations of major elements in bauxites normalized to average fresh parental basalt values *vs*. depth for Cowlitz (upper) and Columbia (bottom) drill cores.

4. Results

All the major and trace element data are listed in **S2.** As a result of extreme weathering, major elements such as Na, Mg, Si, K, and Ca are severely depleted relative to fresh basalts in both profiles; in contrast, Al, Fe, and Ti are enriched (see **Fig. 2**). Alkaline earth metals, such as Sr and Ba display even larger depletion compared with alkali metals like Li and Rb. In general, element depletions are the strongest in the middle of the profiles, and many mobile elements exhibit higher concentrations towards the surface.

Sentinel Bluffs basalts (SBBs) have K_2O contents ranging from 0.88 to 1.23% (**Table 2**) and display resolvable δ^{41}K variations (-0.66 to -0.31‰). Although the range of δ^{41}K is relatively large for igneous rocks, the average of -0.49‰ is indistinguishable from the value of BSE of -0.48 ± 0.03‰ (Wang and Jacobsen, 2016). Compared with SBBs, Pomona Basalts (PBs) have slightly lower K_2O contents (0.39-0.46%). The δ^{41}K values of Pomona basalts are from -0.59 to -0.51‰, which is also slightly lower than that of BSE. Samples from both aeolian deposits have elevated K_2O contents (1.91% for Portland Hills and 2.14% for Palouse) compared with

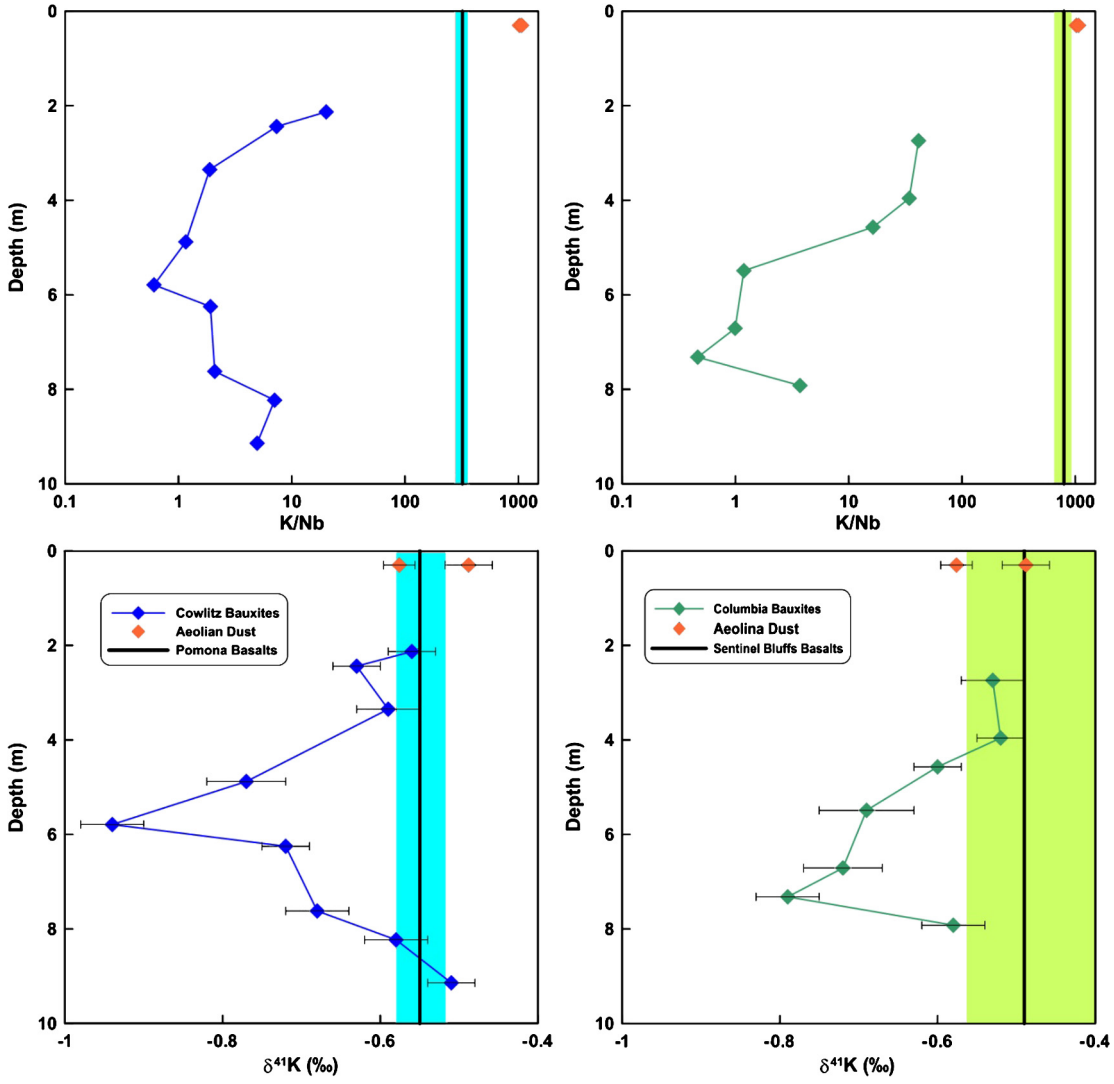

Fig. 3. [K]/[Nb] and δ^{41}K *vs*. depth for Cowlitz bauxites (left, in blue), formed on the Pomona basalts, and Columbia bauxites (right, in green), formed on the Sentinel Bluffs basalts. Bauxites are shown as blue/green diamond symbols and aeolian deposits are shown as orange diamond symbols. The average parent basalt compositions are shown in black lines and rectangular fields show 1se of the average values. Error bars of δ^{41}K represent 2s.e. Data are reported in **Table 2**. (For interpretation of the colors in the figure(s), the reader is referred to the web version of this article.)

Table 2
Potassium isotopic compositions (δ^{41}K) of fresh basalts and aeolian dusts.

Sample	δ^{41}K	n[a]	2s.e.	K_2O (wt.%)[b]	Nb (ppm)[b]	$\frac{K}{Nb}$
Pomona Basalts						
WC-7	-0.54	10	0.02	0.40	10.3	322.2
WC-16	-0.59	10	0.03	0.39	11.1	291.5
WC-21	-0.51	10	0.03	0.46	10.9	350.2
Sentinel Bluffs Basalts						
SB-1	-0.63	11	0.03	1.05	8.4	1037.2
2170	-0.44	11	0.03	0.88	10.3	708.9
2340	-0.31	11	0.02	1.23	12.7	806.7
2370	-0.42	11	0.03	1.09	13.0	695.7
2380	-0.47	11	0.04	1.19	11.9	831.6
2450	-0.66	11	0.03	0.98	11.8	689.4
Aeolian Dust						
PHS-1	-0.58	11	0.02	1.91	15.5	1022.5
Palous-1	-0.49	11	0.03	2.14	16.6	1069.7

[a] *n* = number of repeat measurements by MC-ICP-MS
[b] b. Data are from Liu et al. (2013)

the fresh CRBs. The δ^{41}K values of the aeolian samples (-0.58 and -0.49‰) overlap those of the fresh CRBs, and close to the value of BSE (**Fig. 3**).

As a mobile element, the concentration of K ([K]) is strongly depleted in both profiles relative to fresh basalts. The most [K] depleted samples are in the middle of the profiles. From the middle to the top and bottom of the profiles, the [K] increases (**Fig. 3**). Because the degree of weathering in this study (CIA>98) is more intense compared with most other weathering profiles and little K remains, the bauxites measured here so far have some of the lowest δ^{41}K values among terrestrial rocks. Cowlitz bauxite samples have δ^{41}K ranging from -0.51 to -0.94‰ (**Table 3**). There is a clear correlation between δ^{41}K and K_2O, with the lowest δ^{41}K associated with the lowest K_2O in the middle of the profile (**Fig. 3 and Fig. 4**). The K isotopes of bauxites in the top and bottom profiles are closer to K isotope compositions of fresh basalts and aeolian dusts. Columbia profile also shows a similar trend throughout the profile, although the range of δ^{41}K variation is smaller (-0.52 to -0.79‰). Like K, Li is also an alkali metal elements, and it shows some similarities to K in both profiles, for example the largest [Li] depletions are in the middle of profiles, and the Li is generally enriched in lighter isotopes in bauxites compared with the average of the fresh basalt parents (Liu et al., 2013).

Table 3
Potassium isotopic compositions (δ^{41}K) of drill core bauxites.

Sample	Depth (m)	δ^{41}K	n[a]	2s.e.	K_2O (wt.%)[b]	Nb (ppm)[b]	$\frac{K}{Nb}$	$[K]_{norm}$[c]
Cowlitz Bauxite								
9/3-1	2.13	-0.56	12	0.03	0.15	61.7	20.2	0.063
9/3-2	2.44	-0.63	12	0.03	0.08	90.3	7.4	0.023
9/3-5	3.35	-0.59	12	0.04	0.007	30.8	1.9	0.0059
9/3-9	4.88	-0.77	12	0.05	0.004	28.6	1.2	0.0038
9/3-10	5.79	-0.94	12	0.04	0.003	40.9	0.6	0.0019
9/3-19	6.25	-0.72	12	0.03	0.008	34.7	1.9	0.0059
9/3-21	7.62	-0.68	12	0.04	0.009	35.7	2.1	0.0066
9/3-22	8.23	-0.58	12	0.04	0.03	35.3	7.1	0.022
9/3-23	9.14	-0.51	12	0.03	0.02	33.5	5.0	0.015
Columbia Bauxites								
5/1-4	2.74	-0.53	11	0.04	0.29	58.2	41.3	0.053
5/1-6	3.96	-0.52	11	0.03	0.23	55.8	34.2	0.044
5/1-8	4.57	-0.60	11	0.03	0.16	81.1	16.4	0.021
5/1-10	5.49	-0.69	11	0.06	0.02	139.7	1.2	0.0016
5/1-12	6.71	-0.72	11	0.05	0.01	83.5	1.0	0.0013
5/1-14	7.32	-0.79	11	0.04	0.003	53.5	0.5	0.00064
5/1-15	7.92	-0.58	11	0.04	0.02	44.7	3.7	0.0048

[a] n = number of repeat measurements by MC-ICP-MS
[b] Data are from Liu et al. (2013)
[c] $[K]_{norm}=[K_2O/Nb]_{(bauxite)}/[K_2O/Nb]_{(ave.\ fresh\ basalts)}$; the average K_2O/Nb values of fresh Pomona and Sentinel Bluffs basalts are 321 and 795 respectively

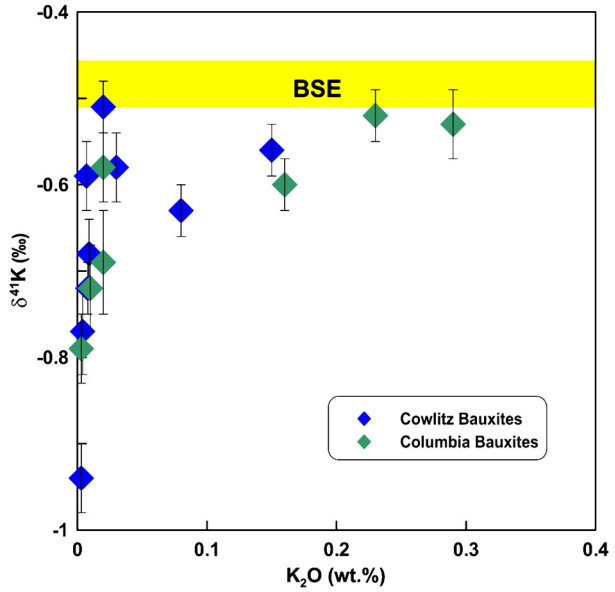

Fig. 4. δ^{41}K *vs.* K_2O content (*wt.%*) in bauxites. Cowlitz bauxites are shown as blue diamond symbols, and Columbia bauxites are shown as green diamond symbols. Yellow field marks δ^{41}K values of the BSE (0.48 ± 0.03‰), according to the calculation by Wang et al. (2016). Error bars on individual data points represent 2s.e.

5. Discussion

5.1. Influence of aeolian dust addition

The bauxite samples in the top 2-5 meters display less depletions in [K] and higher δ^{41}K compared with those in the middle and bottom of the profiles. Previous mineral analysis shows quartz is present from the surface down to ~5 m in both cores, and its abundance decreases progressively with depth (mineralogy and calculated proportions of mineral phases in bauxites are reported in Liu et al. (2013) and summarized in **S3**). There is no presence of quartz below 5 m in either profile. As fresh CRBs do not contain quartz (Hooper and Hawkesworth, 1993), the presence of such mineral is thus the result of aeolian dust deposition at the tops of both profiles**.** Although aeolian deposits in this area show certain heterogeneities in both chemical and isotopic compositions (Liu et al., 2013), they can be negligible considering much larger differences between aeolian dust and basalts as well as weathered products. The abundance of the dust can be determined based on the percentage of quartz and the signature of the Nd isotopes in profiles (less radiogenic near the tops of profiles compared with lower parts, see **S4 and S5**), and Liu et al. (2013) estimated about 30 to 40 *wt.%* dust was added to the top of the bauxite profiles with the proportion of dust decreasing systematically with depth. As the K concentrations in aeolian dusts are about two orders of magnitude higher than in bauxites without aeolian influence, the adding of aeolian dust not only increases the [K] in top profiles but also conceals the K isotopic signature of weathered products. In the top ~5 m of profiles, the [K] decreases significantly with depth, and a good linear correlation between K_2O contents and quartz (*wt.%*) (**Fig. 5A**) indicates that the majority of [K] in top profile is from aeolian dust.

Assuming that all K at the top of the bauxites was added via the dust and K was not lost to leaching following deposition, one can calculate that the K_2O content in the dust should be in the range of 0.2% to 0.9% (see calculation in **S6**). The average K_2O content in nearby aeolian dust is ~2.1 ± 0.3 (2S.D.) % (based on average of two loess samples from research area), much higher than the predicted [K] in the dust by calculation. This discrepancy indicates that K loss through fluid leaching likely occurred during or after aeolian deposition. Assuming the K_2O contents in aeolian dust is 2.1%, about 50% to 90% of total K has been leached out from the dust, which is comparable to the leaching of [Mg] (up to 80%) at the top profile (Liu et al., 2014). In contrast, there is almost no detectable [Li] depletion in the top profile compared with aeolian dusts (Liu et al., 2013), agreeing with the order of mobility (K>Mg>Li) during chemical weathering (Chesworth et al., 1981; Middelburg et al., 1988). In addition, the K isotopic compositions in the top profiles are undistinguishable from those of two aeolian dust samples, indicating limited isotopic fractionation associated with K leaching from the aeolian dust. Previous experiment by Li et al. (2017) has shown that during mineral dissolution, the K isotope fractionations between the solution and minerals ($\Delta^{41}K_{sol\text{-}mil}$) are variable (from negative to positive) and depending on mineralogy. It is possible that the K isotopic fractionation associated with

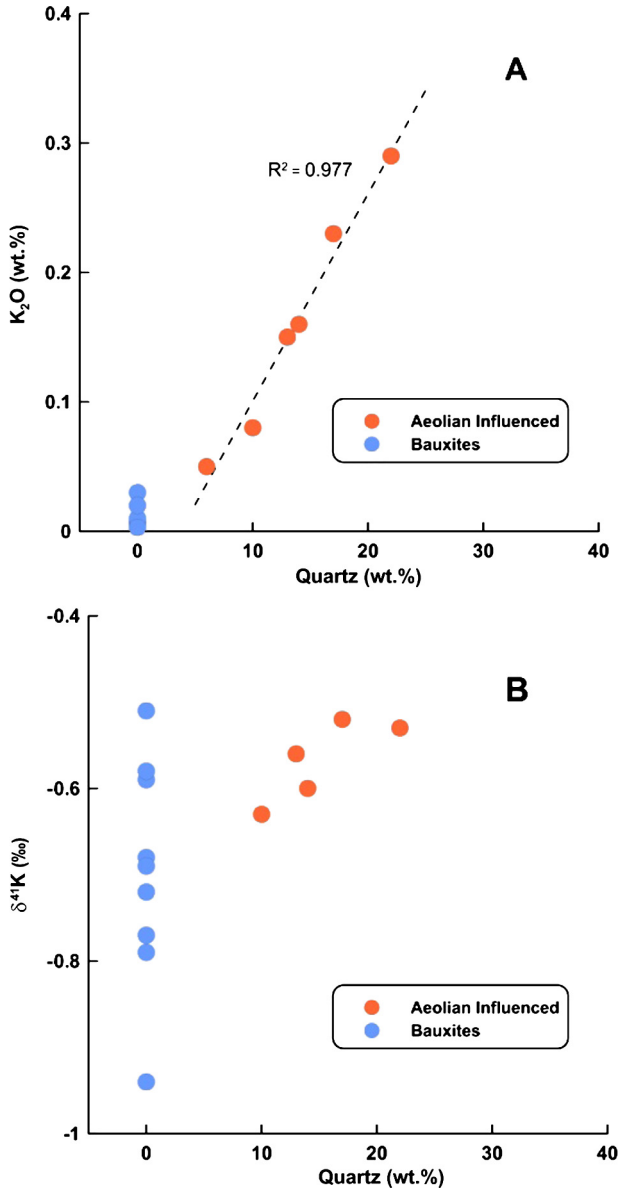

Fig. 5. K_2O (a) and $\delta^{41}K$ (b) *vs*. quartz content (*wt.%*) in bauxites. Bauxites influenced by aeolian addition are identified by orange color. (For interpretation of the colors in the figure(s), the reader is referred to the web version of this article.)

leaching from the aeolian dust is below current analytical uncertainty.

5.2. Factors that control the K fractionation during weathering

Excluding the bauxites affected by the addition of aeolian dusts in the tops, the other weathered products have $\delta^{41}K$ ranging from -0.51 to -0.94‰, systematically lower than the BSE value of 0.48 ± 0.03‰. The isotopically light K compositions of the deeper portions are most likely produced by isotopic fractionation during chemical weathering. For Li and Mg isotopes, the breakdown of primary minerals often leads to isotopic fractionations and possible mechanisms include (1) preferential release of heavy/light isotopes during primary mineral dissolution (Wimpenny et al., 2010) and (2) preferential dissolution of isotopically distinct mineral phases (Ryu et al., 2011). However, isotope fractionation associated with the primary mineral dissolution is unlikely responsible for the K isotopic variations observed in both profiles because all bauxites are the products of intense weathering and are composed entirely of secondary minerals, which include clay minerals, Al and Fe- hydroxides/oxides (see **S3**). The formation of secondary minerals and their interactions with fluid rather than the dissolution of primary minerals should be responsible for the observed large K isotopic fractionation in bauxites compared with the fresh basalts. This is consistent with previous studies on Li, Mg, and Si isotopes, which highlight the importance of secondary minerals in controlling the isotope fractionations of these elements during chemical weathering (Liu et al., 2013; Wimpenny et al., 2010; Ziegler et al., 2005).

To date, there is no experimental study of the K isotopic fractionation associated with exchange between fluid and clay minerals or Al- and Fe-hydroxides/oxides. For such mineral compositions in bauxites, large amount of K^+ is adsorbed onto the surface of minerals (Ghosh and Singh, 2001; Wilson, 2004). Alternatively, K^+ can also enter mineral structures. Due to its large ionic radius of 1.51 Å (Shannon, 1976), when K^+ is incorporated into clay minerals, it predominately occurs at the interlayer sites in 2:1 minerals (*e.g.*, smectite) and only very small amount substitutes octahedral sites in 1:1 (*e.g.*, kaolinite) and 2:1 minerals (Sposito et al., 1999). Like Li^+, bonds in water are stronger than those for K^+ in interlayer and adsorbed onto minerals surfaces (Glendening and Feller, 1995), leading to a preference for heavy K isotopes in water during water-mineral interactions. By contrast, Mg^{2+} commonly has coordination number of six in water and therefore bonds may be similar or weaker than those for Mg^{2+} in octahedral sites in minerals or Mg adsorbed by minerals, leading to the enrichment of light Mg isotopes in water (Tipper et al., 2006; Pogge von Strandmann et al., 2008). The difference in the direction of isotopic fractionation between Mg and K (as well as Li) likely reflects the difference in bond strength between divalent and monovalent cations in minerals *vs*. water.

It should be noted that the role of K^+ varies among different clay minerals as different minerals have various structures and chemical compositions; thus, bond environments for K^+ as well as cation exchange capacities vary. Such differences are likely to produce variable K isotope fractionation factors (α) between fluid and minerals across weathering profiles, because chemical bonding strength is the dominant control on equilibrium isotope fractionation (Schauble, 2004).

5.3. Quantification of K isotope fractionation via Rayleigh modeling

In order to infer the magnitude of the K isotopic fractionation during extreme weathering and compare with other environment, as well as other isotope systems, we use simple Rayleigh fractionation model to quantify the K isotopic fractionation produced by K leaching between fluid and bauxites. Assuming equilibrium fractionation between fluid and bauxites with a constant isotope fractionation factor (α), the fractionation factor α is defined as $\alpha = ({}^{41}K/{}^{39}K)_{fluid}/({}^{41}K/{}^{39}K)_{bauxite}$. Therefore, the Rayleigh fractionation equation can be written as $\delta^{41}K_{bauxite} = (\delta^{41}K_{basalts}+1000)\, f^{(\alpha-1)} - 1000$, where $\delta^{41}K_{bauxite}$ and $\delta^{41}K_{basalts}$ are the K isotopic compositions in the bauxite and fresh basalts, respectively; f is the fraction of K remaining in the residue, calculated from $[K/X]_{bauxite}/[K/X]_{basalt}$ normalized to a chosen immobile element (X). Here we choose X = Nb to normalize other elements in order to evaluate element depletion because Nb is one of the most immobile elements amongst the commonly considered immobile elements (Kurtz et al., 2000; Liu et al., 2013). The K_2O/Nb ratios of Cowlitz and Columbia bauxites are normalized to the average K_2O/Nb value of their fresh parental basalts, Pomona and Sentinel Bluffs basalts respectively. Using the average $\delta^{41}K$ in parental basalts, we model K behavior in bauxites from both profiles (**Fig. 6**), producing an apparent α between 1 and 1.00007.

We notice that bauxite samples in the same profile show slightly different fractionation factors, indicating a simple Rayleigh

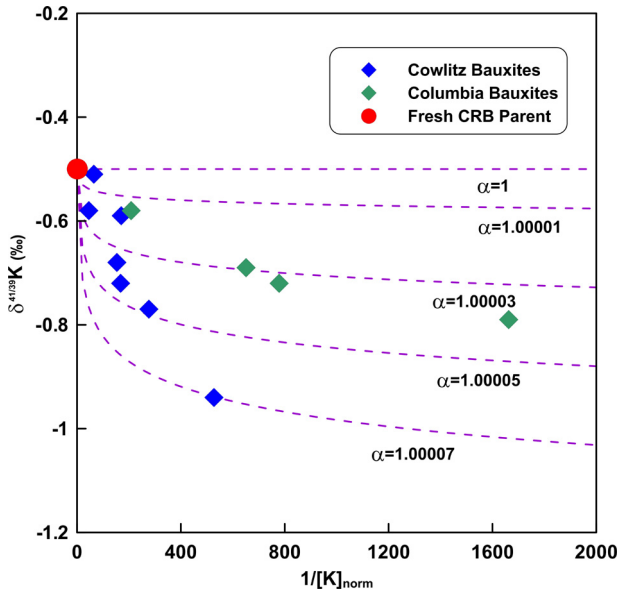

Fig. 6. Rayleigh fractionation model of K isotopic fractionation in the bauxites. $[K]_{norm}$ is defined as $[K]_{norm} = [K_2O/Nb]_{(bauxite)}/[K_2O/Nb]_{(ave.\ fresh\ basalts)}$. All K_2O/Nb values of Cowlitz bauxites (blue) and Columbia bauxites (green) are normalized to the average K_2O/Nb of fresh Pomona basalts and Sentinel Bluffs basalts respectively. The starting material (red dot) has $\delta^{41}K$ of 0.48‰. Bauxites influenced by aeolian dust addition near the top of the profiles are not included. We model K depletion in non-aeolian influenced bauxites via Rayleigh fractionation. The bauxites fit Rayleigh fractionation curves (purple dash lines) with fractionation factors of α, defined as $\alpha = (^{41}K/^{39}K)_{fluid}/(^{41}K/^{39}K)_{bauxite}$.

fractionation process (assuming a constant fractionation factor between the rock and fluid) may not account for all the observed K isotope fractionation in bauxites. The natural processes of weathering are more complex, for example the different secondary mineral phase compositions can lead to variations of fractionation factors (α) through the depth, and the chemical and physical conditions (*e.g.*, temperatures, pH, and reaction rate) of fluid and mineral reaction also change through depths (Brantley et al., 2007; Anderson et al., 2007). As noted by Liu et al. (2014), α inferred by Rayleigh modeling is likely to reflect a combination of dissolution, leaching, and equilibrium partitioning between secondary minerals and pore waters in soils. The K isotope fractionation factors in Columbia bauxites are systematically lower than those in Cowlitz bauxites, reflecting the complexity in chemical weathering systems.

As plotted in diagram of $\delta^{41}K$ *versus* $1/[K]_{norm}$ (**Fig. 6**), the samples display two linear trends. Such linear correlation between isotopic composition and $1/[K]_{norm}$ could result from mixing of two end members, one with high [K] and $\delta^{41}K$ similar to that of basalts, and another one with low [K] and lower $\delta^{41}K$ ($\delta^{41}K$ = -1‰ for Cowlitz and $\delta^{41}K$ = -0.8‰ for Columbia). The first end member could be K from the fresh basalts or aeolian dusts, and the second one could be the secondary mineral phases. If that is the case, all weathered products would have 0.3 to 0.5 ‰ lighter $\delta^{41}K$ than the fresh basalts. However, this is less likely true, since both bauxite profiles are composed entirely of secondary minerals, which include clay minerals, Al and Fe- hydroxides/oxides (see **S3**), and below 5 meters there is no influence of aeolian dust. If it is simple mixing for K, other isotope systems would also display similar correlation on isotope *vs*. 1/[concentration] plots, however Li and Mg do not display such linear trends (Liu et al., 2013, 2014).

5.4. The role of chemical weathering in K global cycle

Once released through the weathering of minerals, K is very soluble and occurs as a simple cation (K^+) over the entire stability field of natural water (Kronberg, 1985). Rivers are the dominant input of the K into the oceans, with majority of the K in river water coming from the weathering of silicate minerals (Berner and Berner, 2012; Sun et al., 2016), therefore, understanding K isotope behavior during continental weathering is critical in determining its riverine input into the oceans.

The major finding of this study is that K in extreme weathering profiles (CIA>98) is isotopically light relative to their parental basalts. This is consistent with a recent study by Li et al. (2019), which revealed that the less weathered river sediments (40<CIA<80) also have lighter K isotopic compositions ($\delta^{41}K$ ranges from -0.74 to -0.48‰) compared with their bed rocks. Although these weathered products developed under different environment and are composed of different secondary minerals, all indicate preferential retention of light K in the continental residue during chemical weathering. Weathered products could thus serve as a low $\delta^{41}K$ end member that contributes to the variations of K isotopic compositions observed in the upper continental crust (Huang et al., in press).

In contrast, dissolved phases of global rivers, which serve as major K input to the oceans, have an average $\delta^{41}K$ of -0.42 ± 0.04‰ (Lee et al., 2018), slightly heavier than the BSE value of -0.48 ± 0.03‰ (Wang and Jacobsen, 2016), and $\delta^{41}K$ of riverine dissolved load generally correlates negatively with the chemical weathering intensity of the drainage basin (Li et al., 2019). It should be noted that K is a nutrient element, therefore, K cycle in biosphere is an important component of its global geochemical cycle (Sardans and Peñuelas, 2015). In principle, two fractionation processes could account for the observed heavy isotope compositions of dissolved K in rivers: (i) weathering of igneous minerals, and (ii) biological utilization of K. To date, there has been no reported study on the role of biological processes on K isotopic composition of surficial waters, however, all available studies point out that the weathered products are the light reservoirs that are complementary to slightly heavier $\delta^{41}K$ in river water. Nevertheless, the K isotopic fractionation during continental weathering is rather small compared with the ~0.6‰ difference between seawater and the BSE $\delta^{41}K$ value. Removal of seawater K occurs via low-temperature hydrothermal alteration, production of authigenic silicates, and cation-exchange with marine sediments (Berner and Berner, 2012). A recent preliminary study reports that $\delta^{41}K$ values of altered basalts (ophiolites with $\delta^{41}K$ between -0.3 and 0.1‰; Parendo et al., 2017) are all higher than the BSE value, which implies that the low-temperature hydrothermal alteration in the oceans is not responsible for enriching heavy $\delta^{41}K$ value in the oceans. Hence, in addition to the K isotopic fractionation during continental weathering, the heavy K isotopic composition in modern seawater should be a combined result of production of authigenic silicates and K exchange processes with marine sediments (see schematic Figure in **S7**).

Solving the isotopic mass balance of K for the modern oceans could place new constrains on its fluxes. The continental runoff (major input) and silicate fixation (major output) dominate the $\delta^{41}K$ budget in seawater, therefore, if fluxes or isotopic compositions of the input and output fluctuated, then the $\delta^{41}K$ of paleo-seawater may be variable outside of analytical uncertainty over geologic time.

6. Conclusions

In this study, we measured K isotopic fractionation during chemical weathering by using a newly developed high-precision K isotope method. The weathered products are from two extremely weathered profiles (drill core bauxites) developed on Columbia River Basalts. Extreme [K] depletion (>98%) and large K isotopic fractionation ($\delta^{41}K$ up to 0.5‰) are observed due to intense chemical weathering.

Both K_2O content and $\delta^{41}K$ show very similar pattern through depths in these two bauxite profiles. The $\delta^{41}K$ values of top profiles are close to the that of aeolian dust as well as fresh basalts. The K isotopic composition of top profiles are modified by the addition of aeolian dust, evidenced by the presence of quartz, less radiogenic Nd, an increase in K_2O, and heavier K isotopic compositions in the upper 5 m compared with deeper bauxites in both profiles. Excluding aeolian dust influenced samples, other bauxites have $\delta^{41}K$ ranging from -0.94 to -0.51 ‰, lower than the value of all fresh basalts and the BSE. The most [K] depleted samples occurred in the middle of the profiles. There is a good correlation between K_2O and $\delta^{41}K$, with the lowest K_2O associated with the lowest $\delta^{41}K$, indicating intense leaching and secondary mineral formation controlling K elemental and isotopic behaviors during weathering. Under the strong chemical weathering conditions, the formation of secondary minerals and their constant interaction with fluid lead to large K isotopic fractionation in bauxites. A simple Rayleigh fractionation model is used to calculate the K isotopic fractionation between fluid and bauxite ($\alpha_{\text{fluid-bauxite}}$), giving α between 1 and 1.00007.

This study reveals that weathering of igneous rocks (basalts in particular) leads to loss of isotopically heavy K from the continents, consistent with the recently reported $\delta^{41}K$ in river and very heavy $\delta^{41}K$ (0.1‰) seen in seawater. However, the K isotopic fractionation during continental weathering itself is insufficient to account for 0.6‰ difference between BSE and the modern seawater.

Declaration of competing interest

We certify that we have NO affiliations with or involvement in any organization or entity with any financial interest (such as honoraria; educational grants; participation in speakers' bureaus; membership, employment, consultancies, stock ownership, or other equity interest; and expert testimony or patent-licensing arrangements), or non-financial interest (such as personal or professional relationships, affiliations, knowledge or beliefs) in the subject matter or materials discussed in this manuscript.

Acknowledgements

H.C. and K.W. thank the McDonnell Center for the Space Sciences at Washington University for their support. X-M.L. acknowledges the support from the University of North Carolina at Chapel Hill. We thank Roberta Rudnick for helpful discussion and Michael Cummings for providing samples. We thank Dr. Louis Derry, Dr. Edward Tipper, and another anonymous reviewer for constructive review.

Appendix A. Supplementary material

Supplementary material related to this article can be found online at https://doi.org/10.1016/j.epsl.2020.116192.

References

Anderson, S.P., von Blanckenburg, F., White, A.F., 2007. Physical and chemical controls on the critical zone. Elements 3 (5), 315–319.
Berner, E.K., Berner, R.A., 2012. Global Environment: Water, Air, and Geochemical Cycles. Princeton University Press, Princeton, N.J.
Brantley, S.L., Goldhaber, M.B., Ragnarsdottir, K.V., 2007. Crossing disciplines and scales to understand the critical zone. Elements 3 (5), 307–314.
Chen, H., Tian, Z., Tuller-Ross, B., Korotev, R.L., Wang, K., 2019. High-precision potassium isotopic analysis by MC-ICP-MS: an inter-laboratory comparison and refined K atomic weight. J. Anal. At. Spectrom. 34 (1), 160–171.
Chesworth, W., Dejou, J., Larroque, P., 1981. The weathering of basalt and relative mobilities of the major elements at Belbex, France. Geochim. Cosmochim. Acta 45 (7), 1235–1243.
Fantle, M.S., Tipper, E.T., 2014. Calcium isotopes in the global biogeochemical Ca cycle: implications for development of a Ca isotope proxy. Earth-Sci. Rev. 129, 148–177.
Frings, P.J., Clymans, W., Fontorbe, G., De La Rocha, C.L., Conley, D.J., 2016. The continental Si cycle and its impact on the ocean Si isotope budget. Chem. Geol. 425, 12–36.
Garrels, R.M., MacKenzie, F.T., 1971. Evolution of Sedimentary Rocks. Norton, New York. 397 pp.
Ghosh, B.N., Singh, R.D., 2001. Potassium release characteristics of some soils of Uttar Pradesh hills varying in altitude and their relationship with forms of soil K and clay mineralogy. Geoderma 104 (1–2), 135–144.
Glendening, E.D., Feller, D., 1995. Cation water interactions - the M(+) (H_2O) (n) clusters for alkali-metals, M = Li, Na, K, Rb, and Cs. J. Phys. Chem. 99 (10), 3060–3067.
Hooper, P.R., Hawkesworth, C.J., 1993. Isotopic and geochemical constraints on the origin and evolution of the Columbia river basalt. J. Petrol. 34 (6), 1203–1246.
Hooper, P.R., 1997. The Columbia river flood basalt provinces, current status. In: Mahoney, J.J., Coffin, M.F. (Eds.), Large Igneous Provinces: Continental, Oceanic, and Planetary Flood Volcanism. American Geophysical Union, Washington, DC, United States, pp. 1–27.
Hu, Y., Chen, X.Y., Xu, Y.K., Teng, F.Z., 2018. High-precision analysis of potassium isotopes by HR-MC-ICPMS. Chem. Geol. 493, 100–108.
Huang, T.Y., Teng, F.Z., Rudnick, R.L., Chen, X.Y., Hu, Y., Liu, Y.S., Wu, F.Y., in press. Heterogeneous potassium isotopic composition of the upper continental crust. Geochim. Cosmochim. Acta. https://doi.org/10.1016/j.gca.2019.05.022.
Kohn, M.J., Miselis, J.L., Fremd, T.J., 2002. Oxygen isotope evidence for progressive uplift of the Cascade Range, Oregon. Earth Planet. Sci. 204 (1–2), 151–165.
Kronberg, B.I., 1985. Weathering dynamics and geosphere mixing with reference to the potassium cycle. Earth Planet. Sci. 41 (2–3), 125–132.
Kurtz, A.C., Derry, L.A., Chadwick, O.A., Alfano, M.J., 2000. Refractory element mobility in volcanic soils. Geology 28, 683–686.
Lee, H., Peucker-Ehrenbrink, K., Chen, H., Hasenmueller, E., Wang, K., 2018. Potassium isotopes in major world rivers: implications for weathering and the seawater budget. In: Goldschmidt Conference.
Li, W.Q., Beard, B.L., Li, S.L., 2016. Precise measurement of stable potassium isotope ratios using a single focusing collision cell multi-collector ICP-MS. J. Anal. At. Spectrom. 31 (4), 1023–1029.
Li, W.Q., Kwon, K.D., Li, S.L., Beard, B.L., 2017. Potassium isotope fractionation between K-salts and saturated aqueous solutions at room temperature: laboratory experiments and theoretical calculations. Geochim. Cosmochim. Acta 214, 1–13.
Li, S., Li, W., Beard, B.L., Raymo, M.E., Wang, X., Chen, Y., Chen, J., 2019. K isotopes as a tracer for continental weathering and geological K cycling. Proc. Natl. Acad. Sci. USA 116 (18), 8740–8745.
Liu, X.M., Rudnick, R.L., 2011. Constraints on continental crustal mass loss via chemical weathering using lithium and its isotopes. Proc. Natl. Acad. Sci. USA 108 (52), 20873–20880.
Liu, X.M., Rudnick, R.L., McDonough, W.F., Cummings, M.L., 2013. Influence of chemical weathering on the composition of the continental crust: Insights from Li and Nd isotopes in bauxite profiles developed on Columbia river basalts. Geochim. Cosmochim. Acta 115, 73–91.
Liu, X.M., Teng, F.Z., Rudnick, R.L., McDonough, W.F., Cummings, M.L., 2014. Massive magnesium depletion and isotope fractionation in weathered basalts. Geochim. Cosmochim. Acta 135, 336–349.
Ludwig, W., Probst, J.L., Kempe, S., 1996. Predicting the oceanic input of organic carbon by continental erosion. Glob. Biogeochem. Cycles 10 (1), 23–41.
Meybeck, M., 1987. Global chemical weathering of surficial rockss estimated from river dissolved loads. Am. J. Sci. 287 (5), 401–428.
Middelburg, J.J., Vanderweijden, C.H., Woittiez, J.R.W., 1988. Chemical processes affecting the mobility of major, minor and trace-elements during weathering of granitic-rocks. Chem. Geol. 68 (3–4), 253–273.
Morgan, L.E., Ramos, D.P.S., Davidheiser-Kroll, B., Faithfull, J., Lloyd, N.S., Ellam, R.M., Higgins, J.A., 2018. High-precision K-41/K-39 measurements by MC-ICP-MS indicate terrestrial variability of delta K-41. J. Anal. At. Spectrom. 33 (2), 175–186.
Nesbitt, H.W., Young, G.M., 1989. Formation and diagenesis of weathering profiles. J. Geol. 97 (2), 129–147.
Parendo, C.A., Jacobsen, S.B., Wang, K., 2017. K isotopes as a tracer of seafloor hydrothermal alteration. Proc. Natl. Acad. Sci. USA 114 (8), 1827–1831.
Pogge von Strandmann, P.A.E., Burton, K.W., James, R.H., van Calsteren, P., Gislason, S.R., Sigfússon, B., 2008. The influence of weathering processes on riverine magnesium isotopes in a basaltic terrain. Earth Planet. Sci. 276 (1–2), 187–197.
Reidel, S.P., 1989. The grande ronde basalt, Columbia river basalt group: stratigraphic descriptions and correlations in Washington, Oregon, and Idaho. In: Volcanism and Tectonism in the Columbia River Flood-Basalt Province. The Geological Society of America, Boulder, CO, pp. 21–45.
Rudnick, R.L., 1995. Making continental crust. Nature 378, 571–578.
Ryu, J.S., Jacobson, A.D., Holmden, C., Lundstrom, C., Zhang, Z.F., 2011. The major ion, delta Ca-44/40, delta Ca-44/42, and delta Mg-26/24 geochemistry of granite weathering at pH=1 and T=25 degrees C: power-law processes and the relative reactivity of minerals. Geochim. Cosmochim. Acta 75 (20), 6004–6026.
Sardans, J., Peñuelas, J., 2015. Potassium: a neglected nutrient in global change. Glob. Ecol. Biogeogr. 24, 261–275.

Schauble, E.A., 2004. Applying stable isotope fractionation theory to new systems. In: Johnson, C.M., Beard, B.L., Albarede, F. (Eds.), Geochemistry of Non-Traditional Stable Isotopes. In: Chantilly, vol. 55. Mineralogical Soc. Amer., pp. 65–111.

Shannon, R.D., 1976. Revised effective ionic-radii and systamtic studies of interatomic distances in halides and chalcogenides. Acta Crystallogr., Sect. A 32 (1), 751–767.

Singer, A., 1980. The paleoclimatic interpretation of clay minerals in soils and weathering profiles. Earth-Sci. Rev. 15, 303–326.

Sposito, G., Skipper, N.T., Sutton, R., Park, S.H., Soper, A.K., Greathouse, J.A., 1999. Surface geochemistry of the clay minerals. Proc. Natl. Acad. Sci. USA 96 (7), 3358–3364.

Suchet, P.A., Probst, J.L., Ludwig, W., 2003. Worldwide distribution of continental rock lithology: implications for the atmospheric/soil CO2 uptake by continental weathering and alkalinity river transport to the oceans. Glob. Biogeochem. Cycles 17 (2), 14.

Sun, X.L., Higgins, J., Turchyn, A.V., 2016. Diffusive cation fluxes in deep-sea sediments and insight into the global geochemical cycles of calcium, magnesium, sodium and potassium. Mar. Geol. 373, 64–77.

Takeuchi, A., Hren, M.T., Smith, S.V., Chamberlain, C.P., Larson, P.B., 2010. Pedogenic carbonate carbon isotopic constraints on paleoprecipitation: evolution of desert in the Pacific northwest, USA, in response to topographic development of the cascade range. Chem. Geol. 277 (3–4), 323–335.

Teng, F.Z., Dauphas, N., Watkins, J.M., 2017. Non-traditional stable isotopes: retrospective and prospective. In: Teng, F.Z., Watkins, J., Dauphas, N. (Eds.), Non-Traditional Stable Isotopes. In: Chantilly, vol. 82. Mineralogical Soc. Amer. & Geochemical Soc., pp. 1–26.

Tipper, E.T., Galy, A., Gaillardet, J., Bickle, M.J., Elderfield, H., Carder, E.A., 2006. The magnesium isotope budget of the modem ocean: constraints from riverine magnesium isotope ratios. Earth Planet. Sci. 250 (1–2), 241–253.

Tolan, T.L., 1989. Revisions to the estimates of the areal extent and volume of the Columbia river basalt group. Geol. Soc. Spec. Pap. 239, 1–20.

Wang, K., Jacobsen, S.B., 2016. An estimate of the bulk silicate Earth potassium isotopic composition based on MC-ICPMS measurements of basalts. Geochim. Cosmochim. Acta 178, 223–232.

Wilson, M.J., 2004. Weathering of the primary rock-forming minerals: processes, products and rates. Clay Miner. 39 (3), 233–266.

Wimpenny, J., Gislason, S.R., James, R.H., Gannoun, A., Pogge Von Strandmann, P.A.E., Burton, K.W., 2010. The behaviour of Li and Mg isotopes during primary phase dissolution and secondary mineral formation in basalt. Geochim. Cosmochim. Acta 74 (18), 5259–5279.

Ziegler, K., Chadwick, O.A., Brzezinski, M.A., Kelly, E.F., 2005. Natural variations of delta Si-30 ratios during progressive basalt weathering, Hawaiian Islands. Geochim. Cosmochim. Acta 69 (19), 4597–4610.